Geophysical Research Letters

RESEARCH LETTER
10.1029/2018GL077476

Key Points:
- SK(K)S splitting parameters were measured along a dense broadband array across the central San Andreas fault
- Anomalous fault-parallel splitting was found for stations located within 35 km east of the San Andreas fault
- The area of fault-parallel splitting may be explained by margin-parallel shear due to a fossil slab translating with the Pacific plate

Supporting Information:
- Supporting Information S1

Correspondence to:
C. Jiang,
chengxinjiang@gmail.com

Citation:
Jiang, C., Schmandt, B., & Clayton, R. W. (2018). An anisotropic contrast in the lithosphere across the central San Andreas fault. *Geophysical Research Letters*, *45*, 3967–3975. https://doi.org/10.1029/2018GL077476

Received 5 FEB 2018
Accepted 20 APR 2018
Accepted article online 30 APR 2018
Published online 9 MAY 2018

An Anisotropic Contrast in the Lithosphere Across the Central San Andreas Fault

Chengxin Jiang[1], Brandon Schmandt[1], and Robert W. Clayton[2]

[1]Department of Earth and Planetary Sciences, University of New Mexico, Albuquerque, NM, USA, [2]Seismological Laboratory, California Institute of Technology, Pasadena, CA, USA

Abstract Seismic anisotropy of the lithosphere and asthenosphere was investigated with a dense broadband seismic transect nearly orthogonal to the central San Andreas fault (SAF). A contrast in SK(K)S splitting was found across the SAF, with a clockwise rotation of the fast orientation ~26° closer to the strike of the SAF and greater delay times for stations located within 35 km to the east. Dense seismograph spacing requires heterogeneous anisotropy east of the SAF in the uppermost mantle or crust. Based on existing station coverage, such a contrast in splitting orientations across the SAF may be unusual along strike and its location coincides with the high-velocity Isabella anomaly in the upper mantle. If the Isabella anomaly is a fossil slab fragment translating with the Pacific plate, the anomalous splitting east of the SAF could indicate a zone of margin-parallel shear beneath the western edge of North America.

Plain Language Summary Directional dependence of seismic wave speeds, referred to as anisotropy, can illuminate preferred orientations or fabrics in the Earth organized by deformation. Seismic anisotropy near the sharply defined central segment of the San Andreas fault was investigated with a new dense temporary seismic transect. A contrast in uppermost mantle anisotropy across the fault was identified, with nearly fault parallel orientations only on the east side of the fault. We suggest that development of asymmetric anisotropy about the central San Andreas may arise due to fault-parallel movement of a fossil slab beneath the western edge of North America.

1. Introduction

Central California provides onshore exposure of a plate boundary with >300 km of right-lateral offset since its Miocene transition from subduction to transform (Atwater & Stock, 1998). Thus, it is an exceptional geodynamic setting in which to investigate interactions between active plate boundary faults, the structural legacy of plate boundary reorganization, and ongoing asthenospheric flow. Geodetic measurements document variations in contemporary strain at the surface near the transform boundary, with the most sharply defined right-lateral shear in the central San Andreas fault (SAF) zone from about the Carrizo Plain to San Juan Bautista (Figure 1; Platt & Becker, 2010; Tong et al., 2013). The distribution of deeper strain is more obscure. Low-frequency earthquakes indicate that a fault-like interface extends almost vertically through the lower crust beneath parts of the central SAF (Shelly, 2017). At greater depth, a contrast in a seismic interface thought to be the lithosphere-asthenosphere boundary suggests that a <50-km-wide shear zone extends through the mantle lithosphere of central California (Ford et al., 2014). Within and beneath the lithosphere, constraints on seismic anisotropy provide insight into the past and present organization of strain, including evidence for remnant strain-induced fabric from subduction (Ozacar & Zandt, 2009) and ongoing asthenospheric flow patterns linked to large-scale mantle circulation (Becker et al., 2006; Silver & Holt, 2002).

Studies of teleseismic shear wave splitting in central California have evolved with increasing availability of broadband data from long-term networks and temporary arrays including EarthScope's Transportable Array (TA), which provided regular ~70 km spacing stations connecting denser arrays (Figure 1; Bonnin et al., 2010; Hartog & Schwartz, 2001; Liu, 2009; Özalaybey & Savage, 1995; Silver & Savage, 1994). Most station-averaged SK(K)S splitting orientations are ~E-W, and near coastal stations in central California exhibit a small clockwise rotation toward the strike of Pacific-North America relative motion (Becker et al., 2012). Multiple studies on back azimuthal variability of splitting have suggested that near the SAF in central California, the station-average splitting orientations result from the combined effects of an ~E-W fast orientation in a thicker asthenospheric layer overlain by a thinner lithospheric layer with SAF-parallel fast orientation (Bonnin et al., 2010; Hartog & Schwartz, 2001; Özalaybey & Savage, 1995; Savage & Silver, 1993). Previously compiled

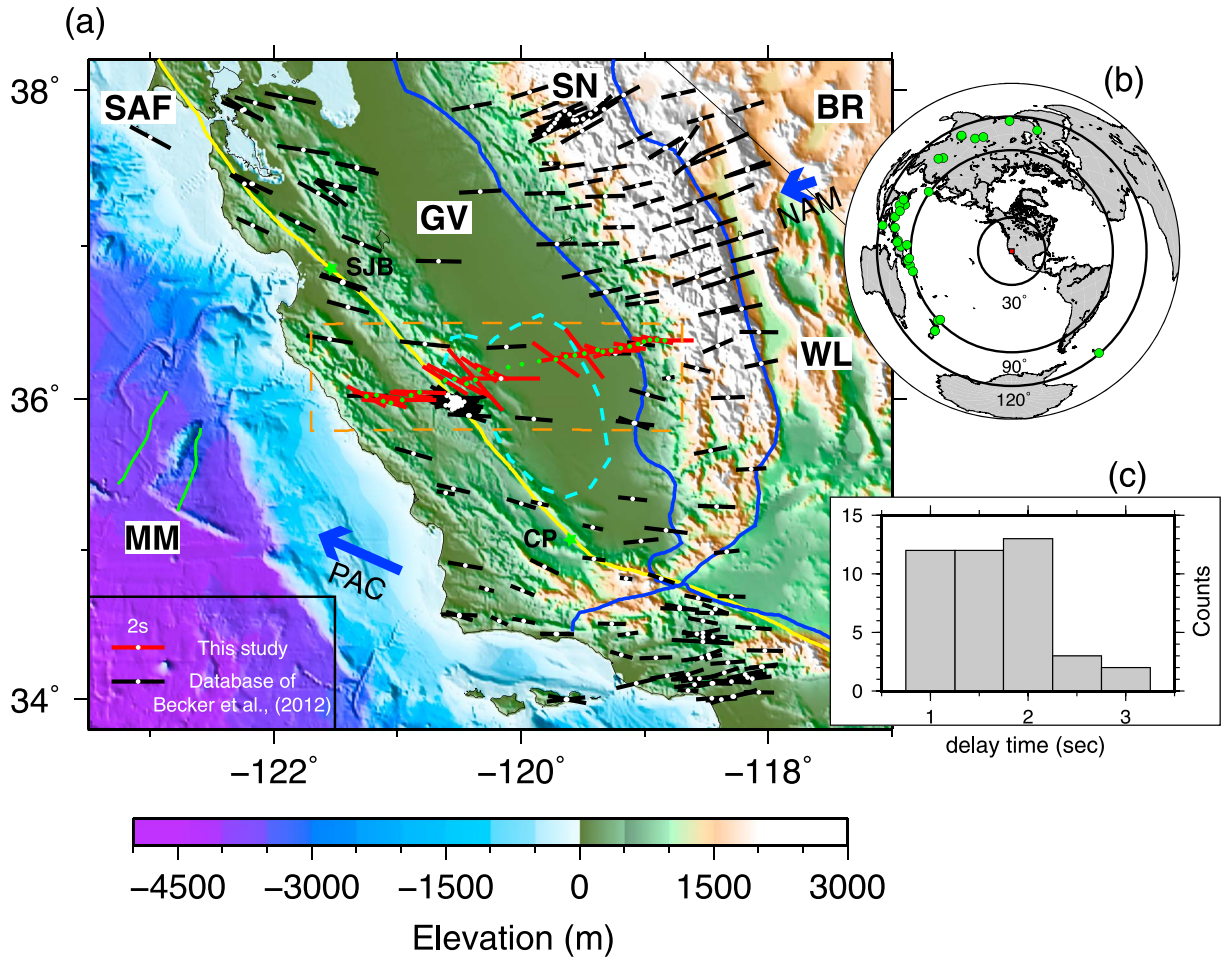

Figure 1. Compiled splitting measurements. (a) The orientation of each bar shows the fast direction with the length indicating the delay time. The red bars with green dots are new measurements, and the black bars with white dots are from Becker et al. (2012). The yellow line denotes the SAF. Two green stars denote San Juan Bautista (SJB) and the Carrizo Plain (CP). The blue lines contour the Sierra Nevada (SN), Great Valley (GV), and Basin and Range province (BR). The green lines offshore show the latest magnetic strips (19–20 Ma) of the Monterey microplate (MM). The dashed cyan circles denote the 4% velocity contour of Isabella anomaly at 60 km depth from Jiang et al. (2018). The blue arrows indicate the Pacific plate (PAC) and North American plate (NAM) motions (Gripp & Gordon, 2002). The dashed orange rectangular outlines the location for Figures 2 and 3a. (b) The distribution of teleseismic events selected for SKS splitting. (c) The distribution of SKS splitting times from the CCSE.

station-average splitting measurements do not exhibit abrupt variations across the SAF in central California (Figure 1). However, changes in splitting parameters over short distances near the southern SAF were recently identified by a dense seismic transect (Barak & Klemperer, 2016).

Here we present new teleseismic shear wave splitting constraints using a dense temporary array that stretches from the coast to the western Sierra Nevada foothills (Figure 1). The strike of the transect is ~75° counterclockwise relative to the strike of the SAF, and average station spacing is ~7 km. Using the new teleseismic data, we identify a contrast in anisotropy across the central SAF and evaluate possible origins of the contrast, including why it may be unusual along strike.

2. Data and Methods

The waveforms used for splitting analysis are from the Central California Seismic Experiment's broadband array (Central California Seismic Experiment (CCSE), 2013; Jiang et al., 2018), whose primary component is transect of 38 broadband seismographs operated for ~18 months in 2013–2015 (Figure 1a). Waveforms from seven nearby permanent stations surrounding the CCSE array were also examined to ensure our splitting

analysis generated results consistent with previous studies. The key benefits of the new measurements are their density and nearly orthogonal orientation to the plate boundary.

We selected waveforms from events with $M_w > 5.8$ and epicentral distance between 88° and 130°. Seismograms were rotated into L-Q-T components (Vinnik, 1977), and band-pass filtered between periods of 10–50 s. Visual inspection was initially used to identify earthquakes that generated coherent SKS or SKKS phases at multiple stations. For the selected events, only phases with signal-to-noise ratio (SNR; defined in Table S1) greater than 2 were considered for splitting analysis. Figure 1b shows the back azimuthal coverage of the 29 selected events.

Shear wave splitting measurements rely on the fact that a shear wave traveling through an anisotropic medium will split into two orthogonally polarized waves traveling at different speeds, creating a delay time between the two arrivals (e.g., Long & Silver, 2009; Nicolas & Christensen, 1987). The fast polarization orientation (ϕ) and delay time (δt) are the two parameters used to characterize the orientation and magnitude of splitting caused by the anisotropic medium. In this study, the two splitting parameters were estimated using the SplitLab software (Wüstefeld et al., 2008). We focused on the method of Silver and Chan (1991), hereafter referred to as the SC method, because this method is better suited for modest SNR waveforms compared to the rotation-correlation method (e.g., Wüstefeld & Bokelmann, 2007), and our limited back azimuthal coverage is not well suited to the splitting intensity method of Chevrot (2000). The SC method conducts a grid-search over the ϕ domain (from $-90°$ to 90° with a step of 2°) and δt domain (from 0 to 4 s with a step of 0.2 s) to find the pair of parameters that minimizes the transverse component energy. A *F* test based method (Walsh et al., 2013) was used to estimate the measurement uncertainties. Figure S1 shows an example SKS splitting measurement from the CCSE array.

We applied objective quality-control metrics to select acceptable splitting measurements following Liu and Gao (2013) and Huang et al. (2015). Figure S2 displays the culling criteria, including SNR of the filtered waveforms, the angular difference between ϕ and event back azimuth, and T-to-Q amplitude ratios before and after the shear-wave splitting analysis (defined in Table S1). Tests with different culling thresholds did not change the major results (Figures S3–S5).

3. Results

The splitting analysis and quality-control procedures yielded a total of 209 acceptable splitting measurements plus 129 acceptable null observations for the 38 CCSE stations. Splitting results for the included seven permanent stations were in close agreement with those from the splitting database of Becker et al. (2012), with a mean difference of 2.52° for the fast orientations and 0.06 s for the delay times. The similarity of the two independent measurements indicates the robustness of the regional splitting pattern and verifies the analysis in this study.

To obtain the final station-average splitting parameters, we averaged the energy surfaces of the accepted splitting measurements (Wolfe & Silver, 1998) and discarded stations with <3 accepted splitting measurements. A station was classified as a null if it has >3 accepted null measurements and <3 nonnull measurements. In general, the stations adjacent to the coast, within ~10 km of the SAF, and in the central-to-western Great Valley have fewer accepted measurements than the rest stations (Figure 2a). The fraction of null measurements is highest in the western Great Valley and lowest near the SAF (Figure 2b). Rose diagrams showing the fast direction of individual good nonnull measurement for CCSE stations is plotted in Figure S6.

Figure 1a displays the station-averaged splitting results across the CCSE array and regional measurements compiled by Becker et al. (2012). The new splitting results display systematic variations along the transect. The fast orientation is nearly E-W west of the SAF, with an averaged splitting time ~1.8 s. East of the SAF the splitting orientations rotate to ~NW-SE directions, almost parallel to the SAF. The averaged splitting time for stations within 35 km east of the SAF is ~2.3 s, which is greater than the average within the same distance west of the SAF. However, the splitting time estimates exhibit greater scatter than the orientations, particularly east of the SAF (Figures S4 and S5). Further to the east, the fault-parallel fast direction is interrupted in the western Great Valley, where there are few acceptable measurements and a high fraction of null splitting (Figures 2a and 2b). In the eastern Great Valley, the fast orientation is approximately E-W, except for two stations (Figure 3a). The average splitting time east of the axis of the Great Valley is ~1.7 s.

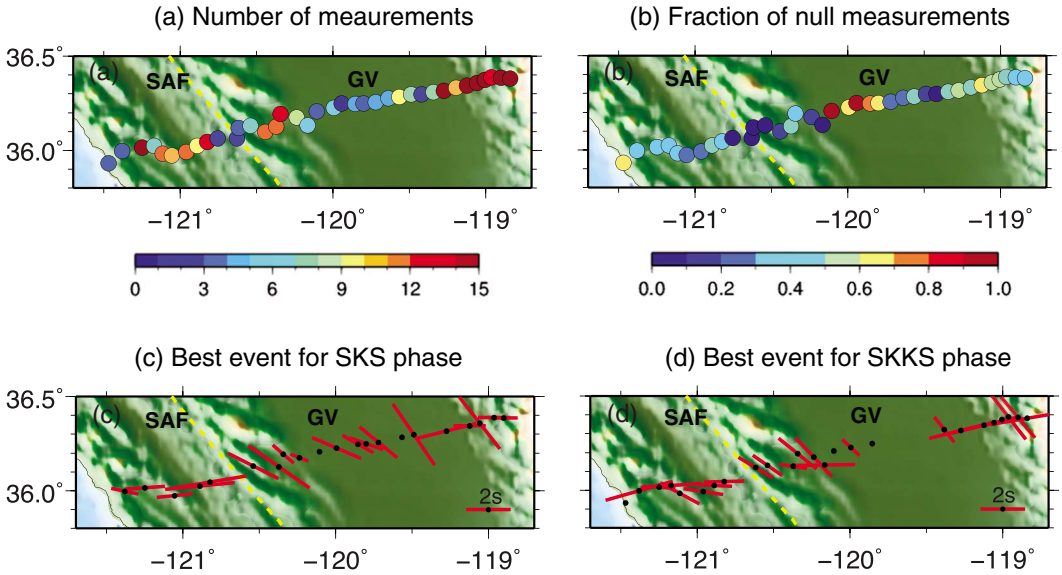

Figure 2. Splitting measurements along the CCSE transect. (a) The total number of selected splitting measurements at CCSE stations including null and nonnull ones. (b) The fraction of null measurements at each station. (c) The best event for SKS splitting measurements. (d) Same as c but for SKKS. The best SKS and SKKS splitting measurements are from the same event.

The variability of the splitting parameters over a short distance near the SAF is well constrained because of the dense array spacing. The contrast across the SAF is expressed in the station-average results (Figures 3a and 3b) and single-event results for both SKS and SKKS phases (Figures 2c and 2d). The distributions of fast orientations for individual splitting measurements within 35 km west and east of the fault cluster at two distinct peaks with averages of 94° and 120°, which were computed after removing 2–3 outliers beyond 2 standard deviations, and if the outliers are retained, the difference decreases by 4°. A Welch's *t* test was applied to test the null hypothesis that measurements on each side of the SAF are drawn from the same population, and we found that the null hypothesis could be rejected with 99% confidence (Welch, 1947). The ~26° clockwise rotation in splitting orientation and the increment of delay time indicate an additional zone of anisotropy just east of the SAF with a fast orientation close to the strike of the SAF. A zoomed-in look at the fast directions at the SAFOD sites shows an average of ~105° (Figure S7), which is intermediate to the averaged fast directions of 94° and ~120° observed on the two sides of SAF.

4. Discussion

4.1. Regional Context for CCSE Splitting

From Figures 1a and 2b, we infer four zones of upper mantle anisotropy. About 65% of the CCSE array exhibits splitting results that match the regional E-W pattern resolved by prior studies within 15°, but these stations are split between the western and eastern ends of the transect, and the average delay time is ~1.7 s. In contrast, two interior segments of the CCSE transect exhibit results that would not have been predicted by interpolation of prior measurements. At stations within ~35 km east of the SAF, fast orientations are dominantly NW-SE and the average delay time is greater, ~2.3 s. Further to the east, an adjacent series of five stations in the western Great Valley produced high fraction of null measurements (Figure 2b). Thus, we expect that the results from the eastern and western ends of the transect reflect regional-scale anisotropic structure that is locally interrupted or overprinted on the east side of the SAF.

The depth of origin for the regional splitting pattern in central California has been dominantly attributed to the asthenosphere, with secondary contributions from the lithosphere leading to back azimuth dependence of individual splitting measurements (Bonnin et al., 2010; Özalaybey & Savage, 1995). The apparent lack of contrast in splitting behaviors across most of the SAF (Figure 1) despite the large structural offset and the modest lithospheric thickness of ~70 km (Ford et al., 2014; Levander & Miller, 2012; Li et al., 2007) make it unlikely that the relatively uniform ~E-W splitting orientation and ~1.5–2 s of delay time are dominantly

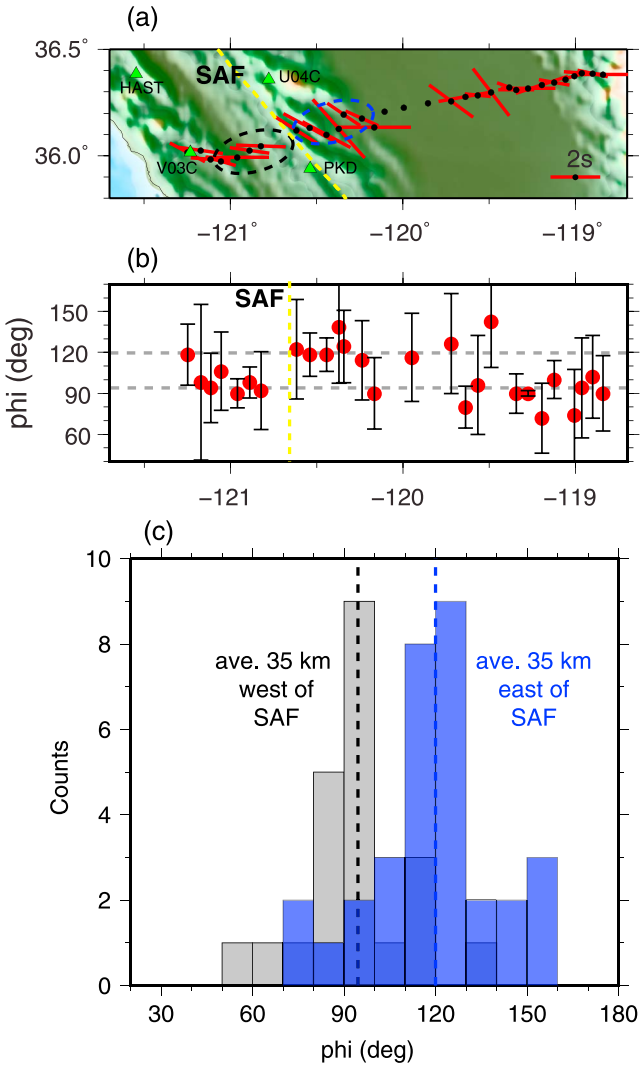

Figure 3. Single-station averaged splitting parameters. (a) The two dashed circles outline stations within 35 km west (black) and east (blue) of SAF. The green triangles denote the stations referred to in section 4.2. (b) Fast direction uncertainties based on the good nonnull measurements at each station. Two grey dashed lines are the averaged fast direction within the two circles in Figure 3a. (c) The fast direction distributions from stations located within the two circles of Figure 3a.

accumulated within the lithosphere. The general ~E-W orientations are consistent with asthenospheric flow directions from mantle circulation models (e.g., Becker et al., 2006). Our results at the eastern and western ends of the CCSE array fit well in this context, so the following sections focus on the newly identified exceptions.

4.2. Contrast in Splitting Across the SAF

Dense arrays afford resolution of changes in anisotropic parameters over short horizontal distances and insight into plausible depths of heterogeneous anisotropy due to Fresnel zone expansion with depth (e.g., Aragon et al., 2017; Barak & Klemperer, 2016; Rümpker et al., 2003). The sharpness of the change in splitting signals west and east of the SAF (Figure 3) indicates distinct anisotropy in the lithosphere because of the largely overlapping Fresnel zones of the ~10 s period shear waves at depths greater than ~70 km (Figure 4d). The average separation distance of ~30 km between the two groups of stations shown in Figure 3 corresponds to >65% Fresnel zone overlap at depths >70 km (Figure 4d), assuming Fresnel zone dimensions for a uniform velocity medium (Spetzler & Snieder, 2004). It should be noted that strong heterogeneities or interfaces that are likely near active plate boundaries would complicate the distribution of sensitivity within the Fresnel zone (e.g., Long et al., 2008). However, the contrast in splitting found across the central SAF clearly differs from numerical splitting predictions for a hypothetical plate boundary model containing a symmetric lithospheric shear zone centered on the SAF (Bonnin et al., 2012). The new results indicate that lithospheric anisotropy is asymmetric about the SAF.

Our inference of a distinct source of anisotropy in the lithosphere near and just east of the SAF at ~36°N is consistent with the splitting results from Bonnin et al. (2010), who used long-term network and TA stations to investigate layered anisotropy. The best fitting model from Bonnin et al. (2010) shows that two stations (U04C and PKD in Figure 3a) located at and just east of the SAF within ~20 km of our array require two layers of anisotropy, with a fault-parallel fast direction in the shallower layer. In contrast, their stations west of the SAF at ~36°N displayed ~E-W fast orientations (HAST and V03C in Figure 3a) and did not exhibit azimuth dependence. Therefore, the rotation of averaged fast direction toward the strike of SAF is most likely due to anomalous SAF-parallel anisotropy in the lithosphere just east of the SAF.

To further test this hypothesis, we used a simple two-layer model to compare the splitting predictions with our observations on both sides of SAF. Forward splitting calculations were conducted with the MSAT toolkit (Walker & Wookey, 2012). Based on Bonnin et al. (2010), we assumed a 180-km-thick asthenospheric layer of an E-W fast orientation that contributes ~1.5 s of splitting time. For the lithospheric layer, we assumed E-W anisotropy (90°) west of the SAF and SAF-parallel anisotropy (120°) east of SAF based on our new results. The strength and thickness of the lithospheric layer were varied to fit the average splitting measurements. The best fit ting model (Figure S8) has lithospheric contributions of ~0.32 and ~0.73 s west and east of the SAF. The delay time contributions correspond to either a 70-km-thick lithospheric column with uniformly distributed anisotropy of 1.5% and 3.5%, or 30-km layers in the lithospheric mantle with 3.5% and 8.2% anisotropy, respectively. Despite the simplicity of the model, it reproduces some aspects of the limited back azimuthal variations observed with the CCSE array, and fits within the context of prior observational results (e.g., Bonnin et al., 2010; Titus et al., 2007).

The evidence for an exceptionally strong SAF-parallel anisotropy contribution in the lithosphere just east of the SAF from this study motivates evaluation of potential geological origins in the crust and uppermost mantle. Crustal anisotropy has been studied extensively near the SAF at Parkfield about 20 km south of

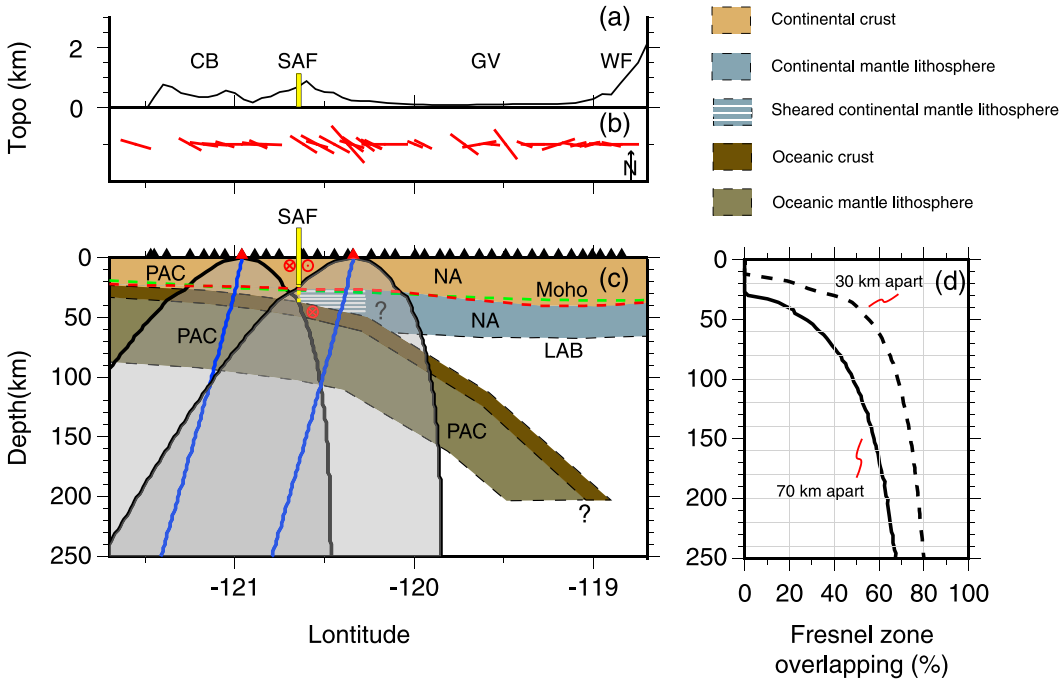

Figure 4. An interpretive cartoon of structural influences on teleseismic spitting. (a) Topography across the CCSE array. Abbreviations include coastal block (CB), Great Valley (GV), and western foothills (WF). The yellow rectangle shows the SAF. (b) A geographic view of station-averaged splitting measurements. (c) Simplified model of Monterey fossil slab following Wang et al. (2013). The black triangles represent CCSE stations. Note that the slab is translating with the Pacific plate (PAC), causing the lithosphere at the western edge of the North American plate (NA) to be sheared. The blue lines are raypaths from a teleseismic event in the west, with grey corridors representing the first Fresnel zone. The dashed green and red lines are Moho depths from Tape et al. (2012) and Schmandt et al. (2015), respectively. The LAB depth is based on the regional average from Ford et al. (2014). Note that the slab is an interpretative cartoon feature. (d) Fresnel zone overlap as a function of depth for 30 and 70 km station separation distances.

the CCSE array (e.g., Cochran et al., 2006) and regionally (Boness & Zoback, 2006). Regionally most crustal fast orientations near the CCSE array are ~SW-NE, consistent with estimates of maximum compressional stress at a high angle to the SAF (Boness & Zoback, 2006). This makes a mid-to-upper crustal origin of the ~SAF-parallel teleseismic splitting unlikely. Receiver function studies sample anisotropy differently, but existing results do not provide evidence for a crustal origin to the change in teleseismic splitting across the SAF. Average crustal fast orientations within ~5 km on both sides of the SAF at Parkfield are generally fault-parallel (Audet, 2015), and the strike of deep crustal fast orientations is ~SW-NE (Ozacar & Zandt, 2009).

In the uppermost mantle beneath the CCSE, seismic tomography images a high-velocity volume that is subhorizontal at ~40–80 km depth beneath much of the coastal block. It begins to dip to the east beneath the North American side of the SAF and extends to ~200 km depth beneath the Sierra Nevada (Jiang et al., 2018; Jones et al., 2014; Wang et al., 2013). This feature is referred to as the Isabella anomaly. Given that both Isabella and the transition of the fast direction from ~E-W to nearly fault-parallel lie at the central segment of the SAF, we consider possible links between the features. Prior to the availability of the TA data the Isabella anomaly was imaged farther east beneath the western Sierra Nevada in the uppermost mantle, and it was almost exclusively hypothesized to be dense foundered arc lithosphere (e.g., Boyd et al., 2004; Zandt et al., 2004). Since TA data improved resolution beneath the Great Valley and continuously along the western plate boundary, the estimated uppermost mantle location of the anomaly has shifted westward, contributing to increasing consideration of an alternative hypothesis that the Isabella anomaly is a fossil slab fragment from Miocene subduction termination (Cox et al., 2016; Pikser et al., 2012; Shelly, 2015; Wang et al., 2013). This fragment would be attached to the Monterey microplate offshore and translating with Pacific plate motion beneath the western edge of the North America (Pikser et al., 2012; Wang et al., 2013). Improved tomographic imaging including the CCSE array data further supports a westward extension of the Isabella anomaly (Jiang et al., 2018).

An important aspect of the fossil slab hypothesis is that just east of the SAF, it predicts that a layer in the uppermost mantle must be sheared between the overlying western edge of North American plate and the

underlying fossil slab moving with the Pacific plate (Figure 4). We propose that this scenario could cause the local rotation of teleseismic splitting orientations east of the SAF (Figure 3). Alternatively, following the foundered lithosphere hypothesis, it is unclear what anisotropic pattern would be predicted on the east side of the SAF, because it depends on the assumed temporal evolution and style of foundering such as a Rayleigh-Taylor drip or delamination-like instability (e.g., Harig et al., 2010; Le Pourhiet et al., 2006; Morency & Doin, 2004). In light of existing results, we favor an explanation that ties the sub-SAF-parallel splitting to plate boundary shear with an unusual along strike expression due to presence of a translating fossil slab (Figure 4). Explanations for anomalous splitting east of the SAF that are not related to the Isabella anomaly may also be viable. For instance, prior studies have explored the possibility of asymmetric mantle viscosity across the SAF (Savage et al., 2004; Teyssier & Tikoff, 1998).

4.3. Null Splitting in the Western Great Valley

Station-average results indicate an area with a high fraction of null splitting in the western Great Valley. The low number of accepted measurements for these stations (Figure 2a) is likely related to high levels of background noise especially for horizontal channels in the Great Valley. However, the high fraction of null measurements is only found for a sequence of five stations in the westernmost Great Valley (Figure 2b). The western Great Valley stations exhibit nulls for events with different back azimuths so not all of the nulls could be caused by back azimuth alignment with the local fast or slow orientation. Consequently, the concentration of null measurements in a small segment of the transect suggests locally heterogeneous shallow structure that interferes with the splitting signal. The western Great Valley is the deepest portion of the basin (~7–10 km), and it is truncated to the west by a steep and actively deforming sediment-basement surface (Wentworth & Zoback, 1989) in contrast to the more gently dipping basement surface of the eastern Great Valley (e.g., Godfrey & Klemperer, 1998). So a simple possibility is that the combination of high background noise reducing the available events plus thick and variably dipping crustal structures may cause the apparent null splitting in the western Great Valley. It is possible that nonnull splitting might be revealed by longer recording durations.

5. Conclusions

New teleseismic shear wave splitting measurements were conducted for a dense broadband transect across the SAF in central California. Most of the resulting splitting orientations and delay times match the regional ~W-E pattern established by sparser station coverage, but ~SAF parallel splitting orientations and larger delay times are found within ~35 km east of the SAF. The anomalous splits indicate a relatively strong and nearly SAF-parallel anisotropy in the lithosphere east of the SAF. The ~SAF-parallel splits are collocated with the along-strike position of the Isabella anomaly, which may represent a fossil slab translating with the Pacific plate and provide a potential explanation for a zone of SAF-parallel shear in the uppermost mantle.

Acknowledgments
CCSE seismic data are publicly available via the IRIS DMC (http://ds.iris.edu/ds/nodes/dmc/), network code TO 2013-2015 (CCSE, 2013). This research was supported by NSF-EAR 1315856 and 1554908, and the seismic instruments used were acquired with support from the Gordon and Betty Moore Foundation. Two anonymous reviewers and the Editor Gavin Hayes are thanked for their constructive feedback.

References

Aragon, J. C., Long, M. D., & Benoit, M. H. (2017). Lateral variations in SKS splitting across the MAGIC array, central Appalachians. *Geochemistry, Geophysics, Geosystems*, *18*, 4136–4155. https://doi.org/10.1002/2017GC007169

Atwater, T., & Stock, J. (1998). Pacific-North America plate tectonics of the Neogene southwestern United States: An update. *International Geology Review*, *40*(5), 375–402. https://doi.org/10.1080/00206819809465216

Audet, P. (2015). Layered crustal anisotropy around the San Andreas fault near Parkfield, California. *Journal of Geophysical Research: Solid Earth*, *120*, 3527–3543. https://doi.org/10.1002/2014JB011821

Barak, S., & Klemperer, S. L. (2016). Rapid variation in upper-mantle rheology across the San Andreas fault system and Salton Trough, southernmost California, USA. *Geology*, *44*(7), 575–578. https://doi.org/10.1130/G37847.1

Becker, T. W., Lebedev, S., & Long, M. D. (2012). On the relationship between azimuthal anisotropy from shear wave splitting and surface wave tomography. *Journal of Geophysical Research*, *117*, B01306. https://doi.org/10.1029/2011JB008705

Becker, T. W., Schulte-Pelkum, V., Blackman, D. K., Kellogg, J. B., & O'Connell, R. J. (2006). Mantle flow under the western United States from shear wave splitting. *Earth and Planetary Science Letters*, *247*(3-4), 235–251. https://doi.org/10.1016/j.epsl.2006.05.010

Boness, N. L., & Zoback, M. D. (2006). Mapping stress and structurally controlled crustal shear velocity anisotropy in California. *Geology*, *34*(10), 825–828. https://doi.org/10.1130/G22309.1

Bonnin, M., Barruol, G., & Bokelmann, G. H. (2010). Upper mantle deformation beneath the North American–Pacific plate boundary in California from SKS splitting. *Journal of Geophysical Research*, *115*, B04306. https://doi.org/10.1029/2009JB006438

Bonnin, M., Tommasi, A., Hassani, R., Chevrot, S., Wookey, J., & Barruol, G. (2012). Numerical modelling of the upper-mantle anisotropy beneath a migrating strike-slip plate boundary: The San Andreas fault system. *Geophysical Journal International*, *191*(2), 436–458. https://doi.org/10.1111/j.1365-246X.2012.05650.x

Boyd, O. S., Jones, C. H., & Sheehan, A. F. (2004). Foundering lithosphere imaged beneath the southern Sierra Nevada, California, USA. *Science*, *305*(5684), 660–662. https://doi.org/10.1126/science.1099181

CCSE (2013). Central California Seismic Experiment. Dataset. Retrieved from https://doi.org/10.7909/C3B56GVW
Chevrot, S. (2000). Multichannel analysis of shear wave splitting. *Journal of Geophysical Research*, *105*, 21,579–21,590. https://doi.org/10.1029/2000JB900199
Cochran, E. S., Li, Y. G., & Vidale, J. E. (2006). Anisotropy in the shallow crust observed around the San Andreas fault before and after the 2004 M 6.0 Parkfield earthquake. *Bulletin of the Seismological Society of America*, *96*(4B), S364–S375. https://doi.org/10.1785/0120050804
Cox, P., Stubailo, I., & Davis, P. (2016). Receiver function and geometric tomography along the Monterey microplate to test slab delamination or lithospheric drip models of the Isabella anomaly, California. *Bulletin of the Seismological Society of America*, *106*(1), 267–280. https://doi.org/10.1785/0120140339
Ford, H. A., Fischer, K. M., & Lekic, V. (2014). Localized shear in the deep lithosphere beneath the San Andreas fault system. *Geology*, *42*(4), 295–298. https://doi.org/10.1130/G35128.1
Godfrey, N. J., & Klemperer, S. L. (1998). Ophiolitic basement to a forearc basin and implications for continental growth: The Coast Range/Great Valley ophiolite, California. *Tectonics*, *17*, 558–570. https://doi.org/10.1029/98TC01536
Gripp, A. E., & Gordon, R. G. (2002). Young tracks of hotspots and current plate velocities. *Geophysical Journal International*, *150*(2), 321–361. https://doi.org/10.1046/j.1365-246X.2002.01627.x
Harig, C., Molnar, P., & Houseman, G. A. (2010). Lithospheric thinning and localization of deformation during Rayleigh-Taylor instability with nonlinear rheology and implications for intracontinental magmatism. *Journal of Geophysical Research*, *115*, B02205. https://doi.org/10.1029/2009JB006422
Hartog, R., & Schwartz, S. Y. (2001). Depth-dependent mantle anisotropy below the San Andreas fault system: Apparent splitting parameters and waveforms. *Journal of Geophysical Research*, *106*, 4155–4167. https://doi.org/10.1029/2000JB900382
Huang, Z., Wang, L., Xu, M., Ding, Z., Wu, Y., Wang, P., et al. (2015). Teleseismic shear-wave splitting in SE Tibet: Insight into complex crust and upper-mantle deformation. *Earth and Planetary Science Letters*, *432*, 354–362. https://doi.org/10.1016/j.epsl.2015.10.027
Jiang, C., Schmandt, B., Hansen, S. M., Dougherty, S., Clayton, R. W., Farrell, J., & Lin, F.-C. (2018). Rayleigh and S wave tomography constraints on subduction termination and lithospheric foundering in central California. *Earth and Planetary Science Letters*, *488*, 14–26. https://doi.org/10.1016/j.epsl.2018.02.009
Jones, C. H., Reeg, H., Zandt, G., Gilbert, H., Owens, T. J., & Stachnik, J. (2014). P-wave tomography of potential convective downwellings and their source regions, sierra Nevada, California. *Geosphere*, *10*(3), 505–533. https://doi.org/10.1130/GES00961.1
Le Pourhiet, L., Gurnis, M., & Saleeby, J. (2006). Mantle instability beneath the Sierra Nevada mountains in California and Death Valley extension. *Earth and Planetary Science Letters*, *251*(1-2), 104–119. https://doi.org/10.1016/j.epsl.2006.08.028
Levander, A., & Miller, M. S. (2012). Evolutionary aspects of lithosphere discontinuity structure in the western US. *Geochemistry, Geophysics, Geosystems*, *13*, Q0AK07. https://doi.org/10.1029/2012GC004056
Li, X., Yuan, X., & Kind, R. (2007). The lithosphere-asthenosphere boundary beneath the western United States. *Geophysical Journal International*, *170*(2), 700–710. https://doi.org/10.1111/j.1365-246X.2007.03428.x
Liu, K. H. (2009). NA-SWS-1.1: A uniform database of teleseismic shear wave splitting measurements for North America. *Geochemistry, Geophysics, Geosystems*, *10*, Q05011. https://doi.org/10.1029/2009GC002440
Liu, K. H., & Gao, S. S. (2013). Making reliable shear-wave splitting measurements. *Bulletin of the Seismological Society of America*, *103*(5), 2680–2693. https://doi.org/10.1785/0120120355
Long, M. D., De Hoop, M. V., & Van Der Hilst, R. D. (2008). Wave-equation shear wave splitting tomography. *Geophysical Journal International*, *172*(1), 311–330. https://doi.org/10.1111/j.1365-246X.2007.03632.x
Long, M. D., & Silver, P. G. (2009). Shear wave splitting and mantle anisotropy: Measurements, interpretations, and new directions. *Surveys in Geophysics*, *30*(4–5), 407–461. https://doi.org/10.1007/s10712-009-9075-1
Morency, C., & Doin, M. P. (2004). Numerical simulations of the mantle lithosphere delamination. *Journal of Geophysical Research*, *109*, B03410. https://doi.org/10.1029/2003JB002414
Nicolas, A., & Christensen, N. I. (1987). Formation of anisotropy in upper mantle peridotites-a review. *Composition, Structure and Dynamics of the Lithosphere-Asthenosphere System*, 111–123. https://doi.org/10.1029/GD016p0111
Ozacar, A. A., & Zandt, G. (2009). Crustal structure and seismic anisotropy near the San Andreas fault at Parkfield, California. *Geophysical Journal International*, *178*(2), 1098–1104. https://doi.org/10.1111/j.1365-246X.2009.04198.x
Özalaybey, S., & Savage, M. K. (1995). Shear-wave splitting beneath western United States in relation to plate tectonics. *Journal of Geophysical Research*, *100*, 18,135–18,149. https://doi.org/10.1029/95JB00715
Pikser, J. E., Forsyth, D. W., & Hirth, G. (2012). Along-strike translation of a fossil slab. *Earth and Planetary Science Letters*, *331*, 315–321.
Platt, J. P., & Becker, T. W. (2010). Where is the real transform boundary in California? *Geochemistry, Geophysics, Geosystems*, *11*, Q06012. https://doi.org/10.1029/2010GC003060
Rümpker, G., Ryberg, T., & Bock, G. (2003). Boundary-layer mantle flow under the Dead Sea transform fault inferred from seismic anisotropy. *Nature*, *425*(6957), 497–501. https://doi.org/10.1038/nature01982
Savage, M. K., Fischer, K. M., & Hall, C. E. (2004). Strain modelling, seismic anisotropy and coupling at strike-slip boundaries: Applications in New Zealand and the San Andreas fault. *Geological Society, London, Special Publications*, *227*(1), 9–39. https://doi.org/10.1144/GSL.SP.2004.227.01.02
Savage, M. K., & Silver, P. G. (1993). Mantle deformation and tectonics: Constraints from seismic anisotropy in the western United States. *Physics of the Earth and Planetary Interiors*, *78*(3–4), 207–227. https://doi.org/10.1016/0031-9201(93)90156-4
Schmandt, B., Lin, F. C., & Karlstrom, K. E. (2015). Distinct crustal isostasy trends east and west of the Rocky Mountain front. *Geophysical Research Letters*, *42*, 10,290–10,298. https://doi.org/10.1002/2015GL066593
Shelly, D. R. (2015). Complexity of the deep San Andreas fault zone defined by cascading tremor. *Nature Geoscience*, *8*(2), 145–151. https://doi.org/10.1038/ngeo2335
Shelly, D. R. (2017). A 15 year catalog of more than 1 million low-frequency earthquakes: Tracking tremor and slip along the deep San Andreas fault. *Journal of Geophysical Research: Solid Earth*, *122*, 3739–3753. https://doi.org/10.1002/2017JB014047
Silver, P. G., & Chan, W. W. (1991). Shear wave splitting and subcontinental mantle deformation. *Journal of Geophysical Research*, *96*, 16,429–16,454. https://doi.org/10.1029/91JB00899
Silver, P. G., & Holt, W. E. (2002). The mantle flow field beneath western North America. *Science*, *295*(5557), 1054–1057. https://doi.org/10.1126/science.1066878
Silver, P. G., & Savage, M. K. (1994). The interpretation of shear-wave splitting parameters in the presence of two anisotropic layers. *Geophysical Journal International*, *119*(3), 949–963. https://doi.org/10.1111/j.1365-246X.1994.tb04027.x
Spetzler, J., & Snieder, R. (2004). The Fresnel volume and transmitted waves. *Geophysics*, *69*(3), 653–663. https://doi.org/10.1190/1.1759451

Tape, C., Plesch, A., Shaw, J. H., & Gilbert, H. (2012). Estimating a continuous Moho surface for the California unified velocity model. *Seismological Research Letters*, *83*(4), 728–735. https://doi.org/10.1785/0220110118

Teyssier, C., & Tikoff, B. (1998). Strike-slip partitioned transpression of the San Andreas fault system: A lithospheric-scale approach. *Geological Society, London, Special Publications*, *135*(1), 143–158. https://doi.org/10.1144/GSL.SP.1998.135.01.10

Titus, S. J., Medaris, L. G., Wang, H. F., & Tikoff, B. (2007). Continuation of the San Andreas fault system into the upper mantle: Evidence from spinel peridotite xenoliths in the Coyote Lake basalt, central California. *Tectonophysics*, *429*(1-2), 1–20. https://doi.org/10.1016/j.tecto.2006.07.004

Tong, X., Sandwell, D. T., & Smith-Konter, B. (2013). High-resolution interseismic velocity data along the San Andreas fault from GPS and InSAR. *Journal of Geophysical Research: Solid Earth*, *118*, 369–389. https://doi.org/10.1029/2012JB009442

Vinnik, L. P. (1977). Detection of waves converted from P to SV in the mantle. *Physics of the Earth and Planetary Interiors*, *15*(1), 39–45. https://doi.org/10.1016/0031-9201(77)90008-5

Walker, A. M., & Wookey, J. (2012). MSAT—A new toolkit for the analysis of elastic and seismic anisotropy. *Computers & Geosciences*, *49*, 81–90. https://doi.org/10.1016/j.cageo.2012.05.031

Walsh, E., Arnold, R., & Savage, M. K. (2013). Silver and Chan revisited. *Journal of Geophysical Research: Solid Earth*, *118*, 5500–5515. https://doi.org/10.1002/jgrb.50386

Wang, Y., Forsyth, D. W., Rau, C. J., Carriero, N., Schmandt, B., Gaherty, J. B., & Savage, B. (2013). Fossil slabs attached to unsubducted fragments of the Farallon plate. *Proceedings of the National Academy of Sciences of the United States of America*, *110*(14), 5342–5346. https://doi.org/10.1073/pnas.1214880110

Welch, B. L. (1947). The generalization of students' problem when several different population variances are involved. *Biometrika*, *34*(1-2), 28–35.

Wentworth, C. M., & Zoback, M. D. (1989). The style of late Cenozoic deformation at the eastern front of the California Coast Ranges. *Tectonics*, *8*, 237–246. https://doi.org/10.1029/TC008i002p00237

Wolfe, C. J., & Silver, P. G. (1998). Seismic anisotropy of oceanic upper mantle: Shear wave splitting methodologies and observations. *Journal of Geophysical Research*, *103*, 749–771. https://doi.org/10.1029/97JB02023

Wüstefeld, A., & Bokelmann, G. (2007). Null detection in shear-wave splitting measurements. *Bulletin of the Seismological Society of America*, *97*(4), 1204–1211. https://doi.org/10.1785/0120060190

Wüstefeld, A., Bokelmann, G., Zaroli, C., & Barruol, G. (2008). SplitLab: A shear-wave splitting environment in Matlab. *Computers & Geosciences*, *34*(5), 515–528. https://doi.org/10.1016/j.cageo.2007.08.002

Zandt, G., Hersh, G., Owens, T. J., Ducea, M., Saleeby, J., & Jones, C. H. (2004). Active foundering of a continental arc root beneath the southern Sierra Nevada in California. *Nature*, *431*(7004), 41–46. https://doi.org/10.1038/nature02847